Supporting Information

Stable Copper-Based Metal-Organic Frameworks Supported Pt-Bi Nanoparticles for Selective Oxidation of Glycerol into Dihydroxyacetone

Liang Lv, Tao Chen, Chaohui Guan, Jing Yu, Yijing Pian, Zihan Ma, Junfeng Du, Shuai Zhang, Hang Wei and Haibin Chu*

Inner Mongolia Key Laboratory of Rare Earth Catalysis, Inner Mongolia Engineering and Technology Research Center for Catalytic Conversion and Utilization of Carbon Resource Molecules, School of Chemistry and Chemical Engineering, Inner Mongolia University, Hohhot 010021, P.R. China

*Corresponding author. E-mail address: chuhb@imu.edu.cn

Table S1. ICP data of Pt and Bi content in Pt-Bi/Cu-MOF, Pt/Cu-MOF, and Pt-Bi/CuO catalysts before and after the cycle.

Sample	Pt% (before)	Bi% (before)	Pt% (after)	Bi% (after)
Pt-Bi/Cu-MOF	4.77	4.71	4.69	4.83
Pt/Cu-MOF	4.56	-	-	-
Pt-Bi/CuO	4.77	4.63	-	-

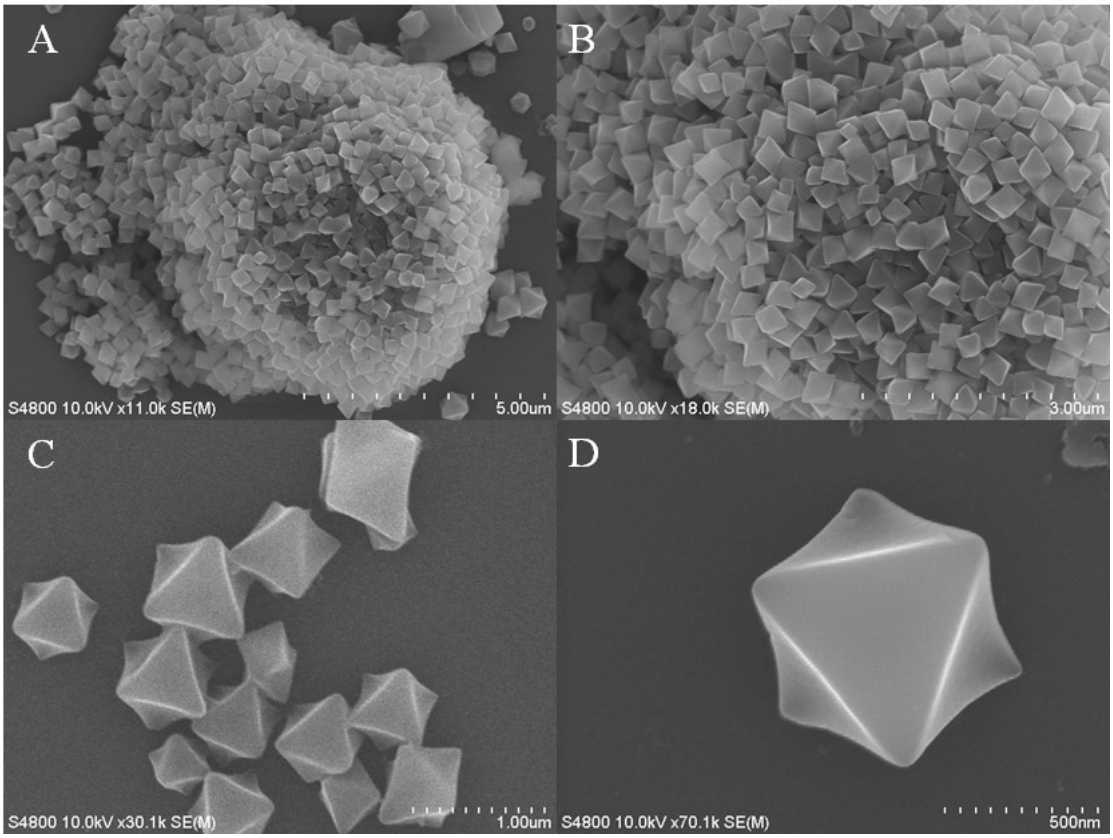

Figure S1. SEM images of Cu-MOF.

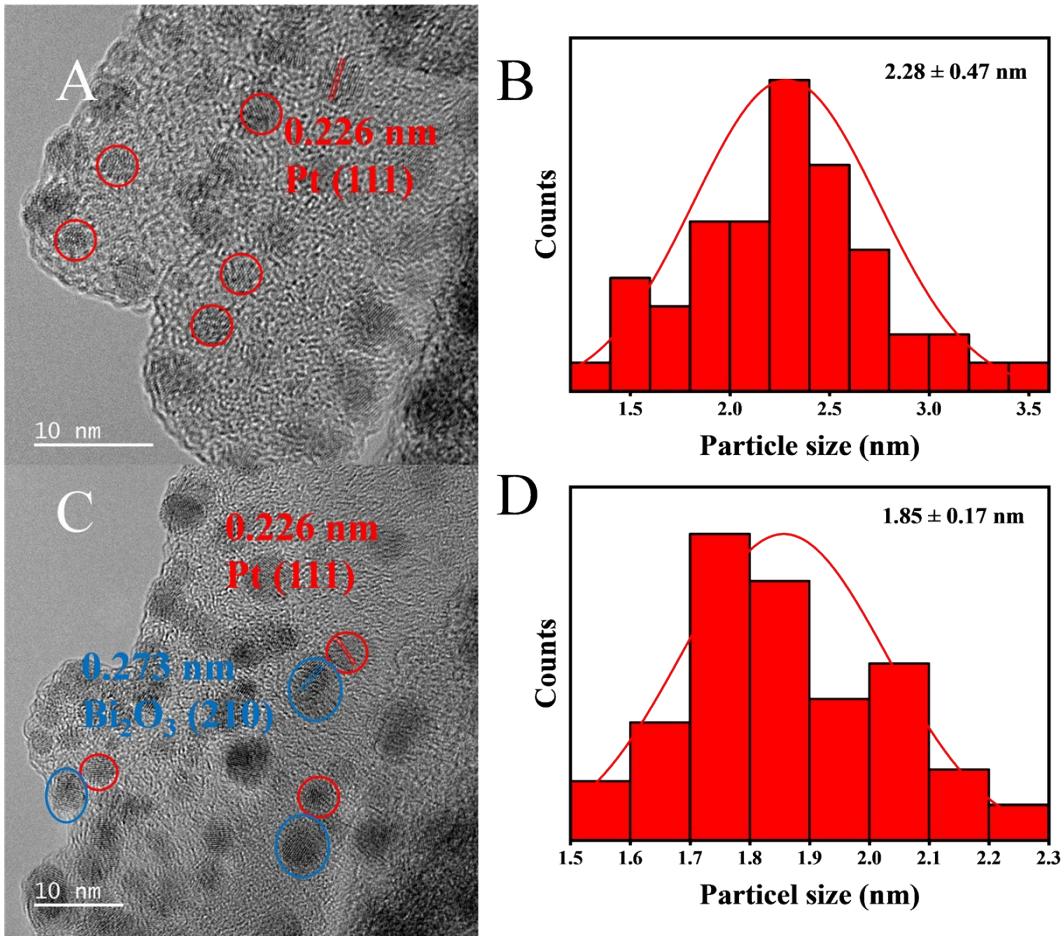

Figure S2. TEM images of (A) Pt/Cu-MOF and (C) Pt-Bi/Cu-MOF catalysts. (B, D) The corresponding size distribution of Pt particles in the catalysts.

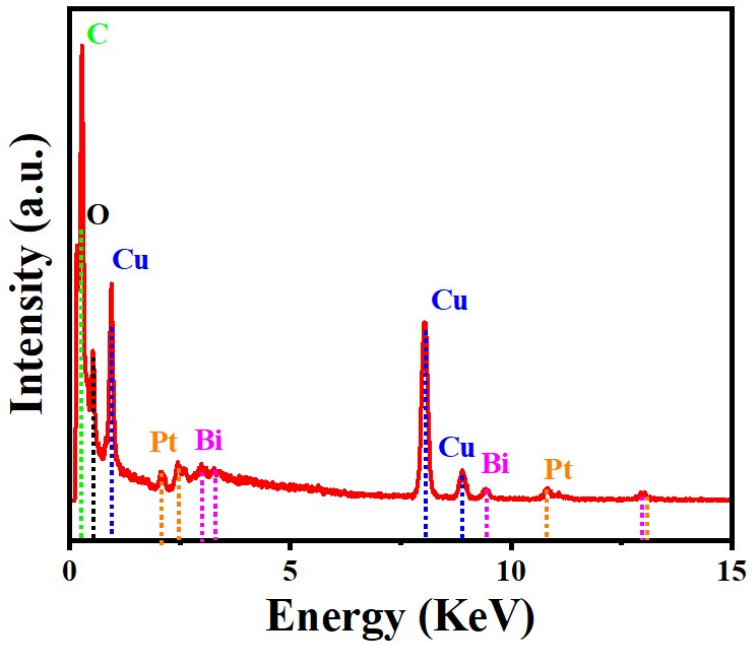

Figure S3. EDS spectrum of Pt-Bi/Cu-MOF catalyst.

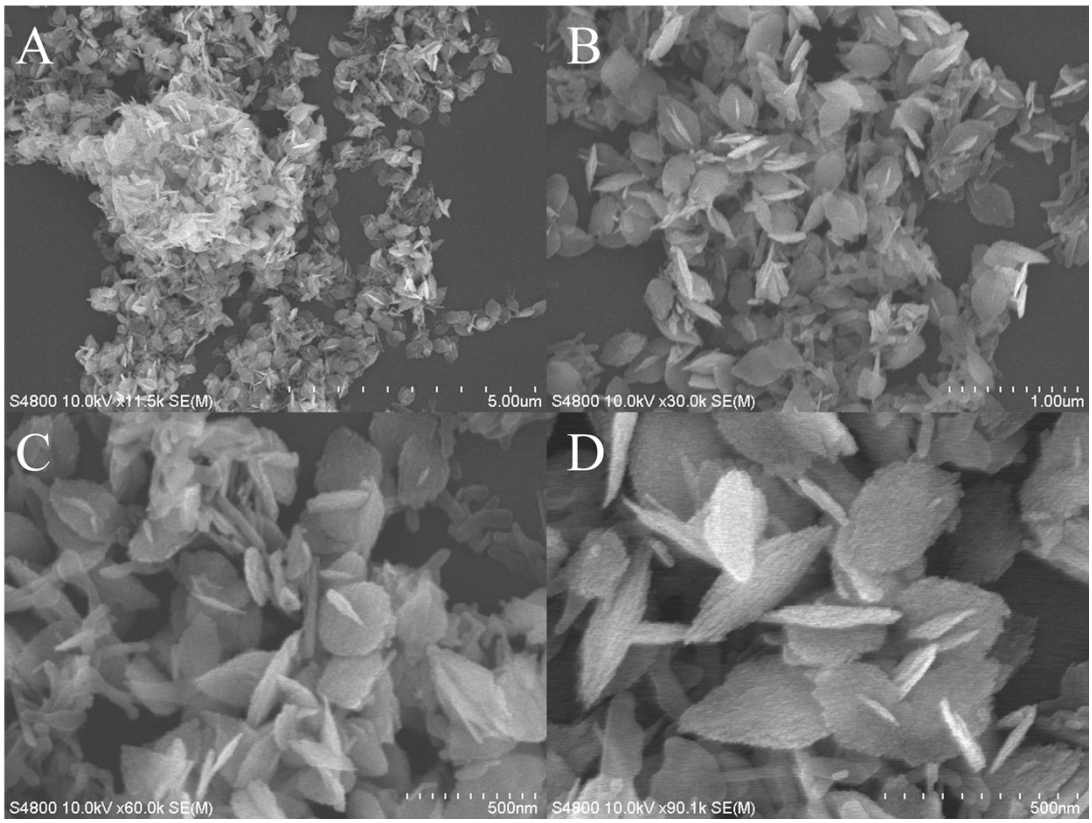

Figure S4. SEM images of CuO.

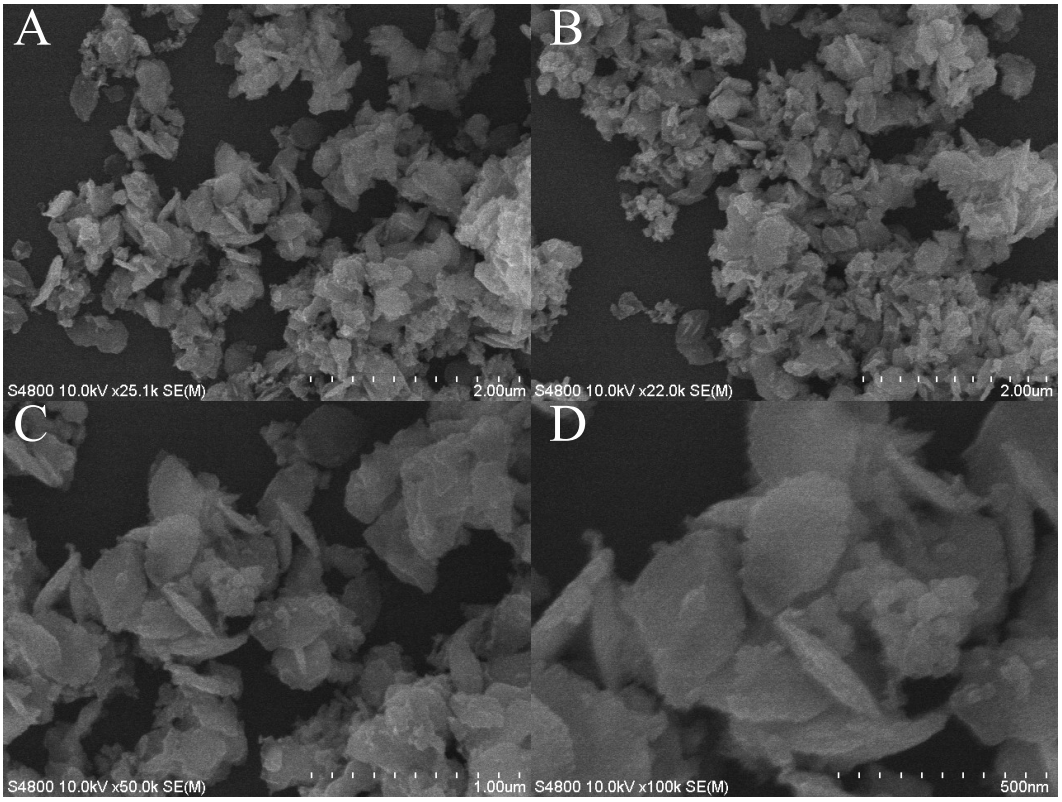

Figure S5. SEM images of Pt-Bi/CuO.

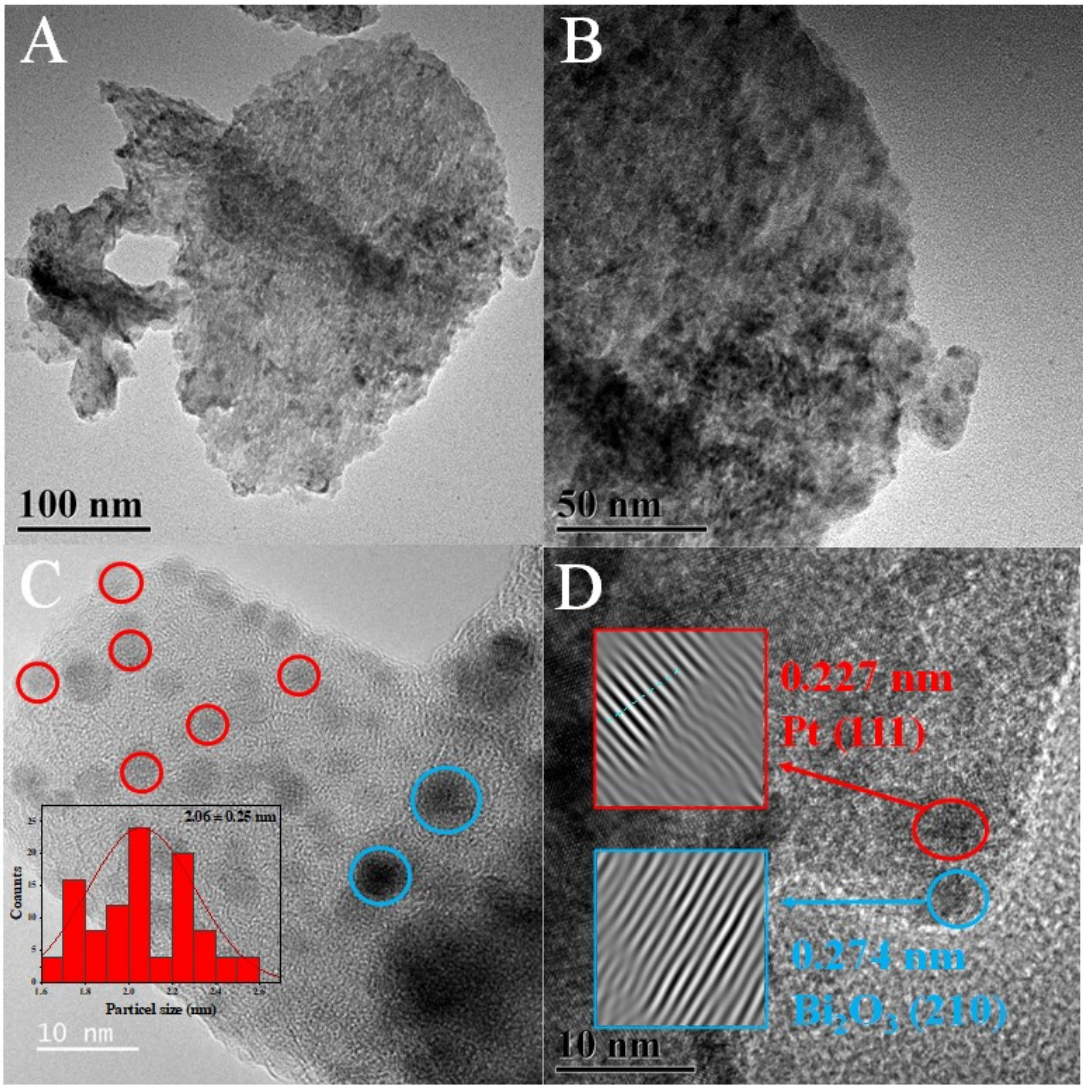

Figure S6. TEM images of Pt-Bi/CuO. The inset in (C) represent the size histogram of Pt nanoparticles.

Table S2. The Cu^{2+} $2p_{3/2}$ peak positions, Cu LMM peak positions, and peak area ratios of the three catalysts.

Sample	Cu^{2+} $2p_{3/2}$	Cu LMM	$S_{satellite\ peak}$: $S_{main\ peak}$
Cu-MOF	935.3 eV	572.1 eV	0.97
Pt/Cu-MOF	934.4 eV	571.2 eV	0.27
Pt-Bi/Cu-MOF	935.7 eV	572.5 eV	0.83

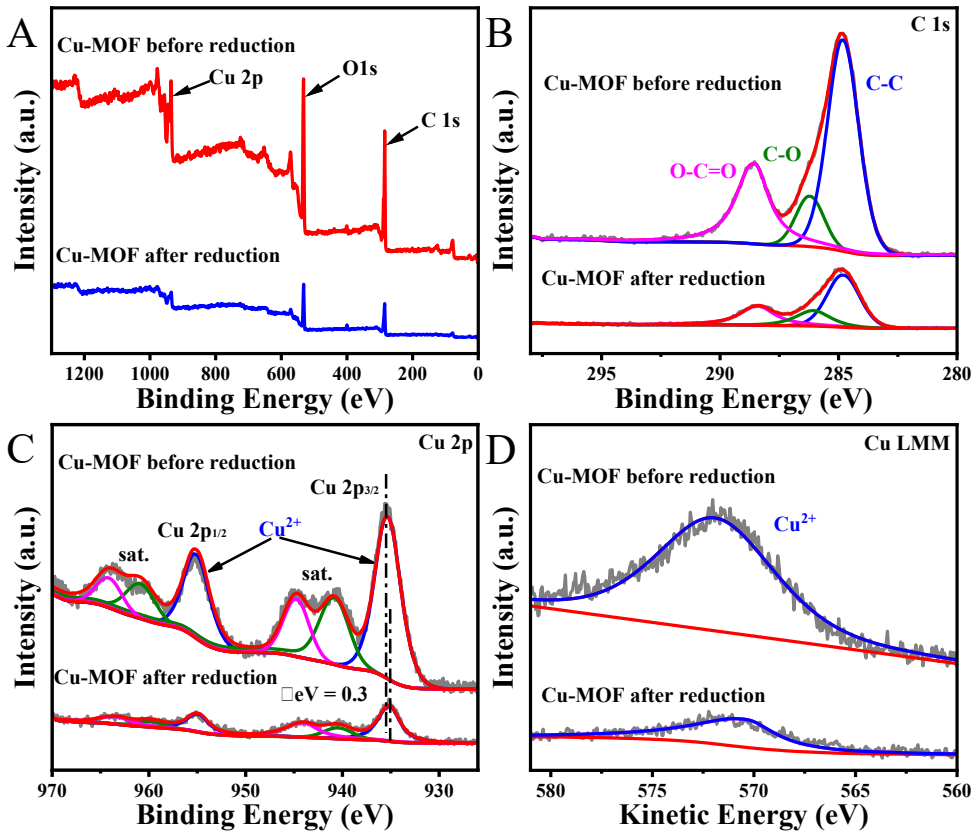

Figure S7. Comparison of XPS spectra of Cu-MOF before and after $NaBH_4$ reduction. (A) survey, (B) C 1s, (C) Cu 2p, and (D) Cu LMM.

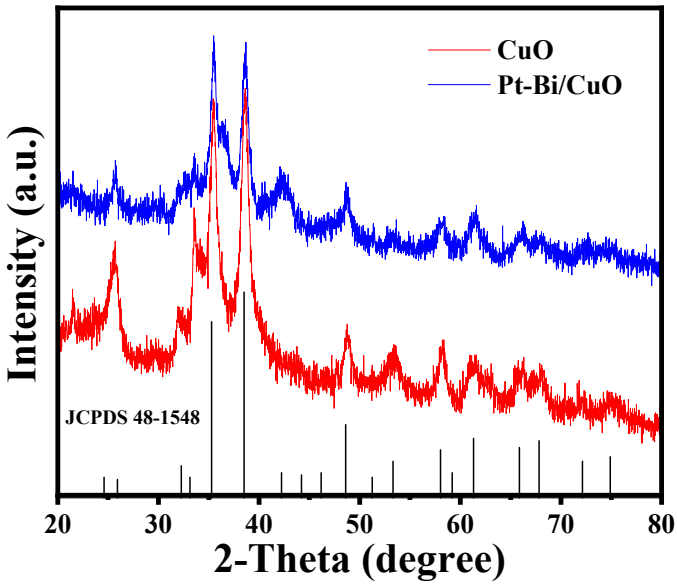

Figure S8. XRD patterns of CuO and Pt-Bi/CuO.

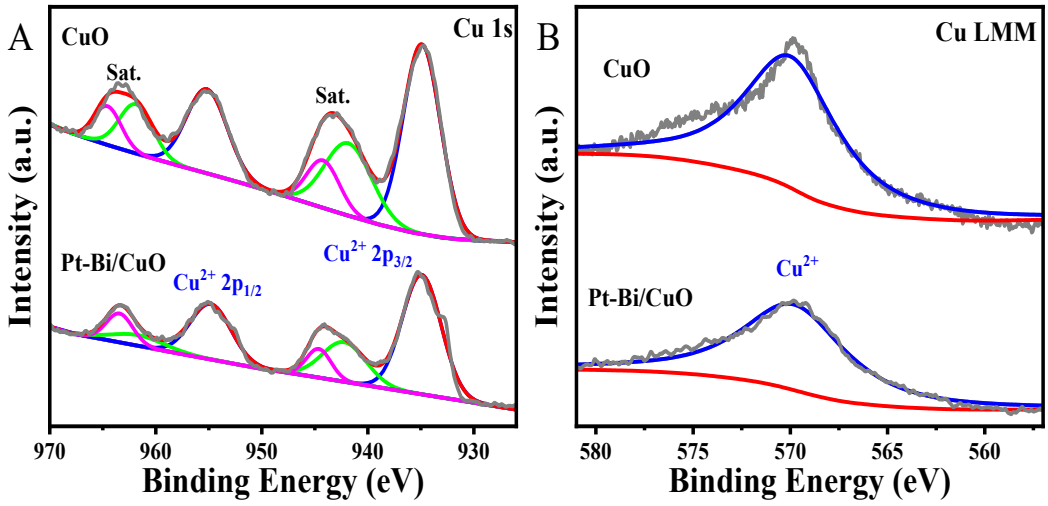

Figure S9. The XPS spectra of (A) Cu 1s and (B) Cu LMM in Pt-Bi/CuO and CuO.

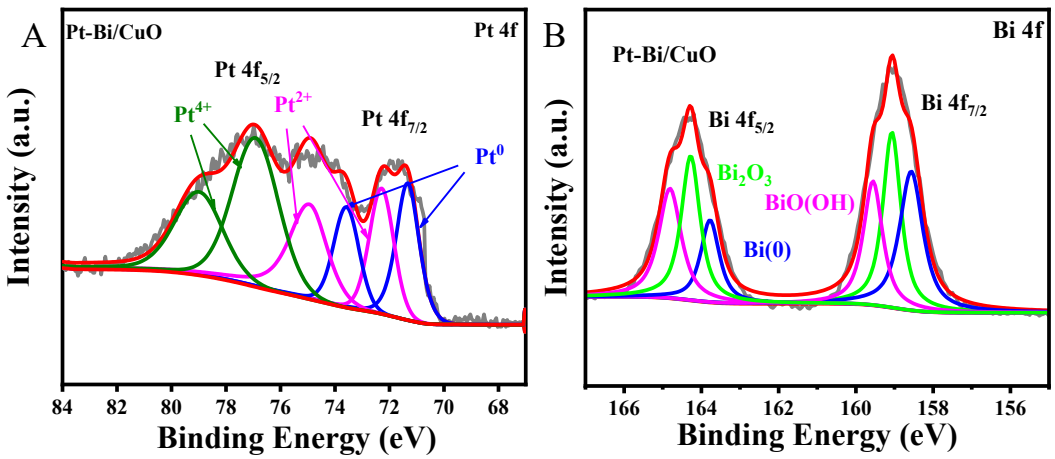

Figure S10. The XPS spectra of (A) Pt 4f and (B) Bi 4f in Pt-Bi/CuO.

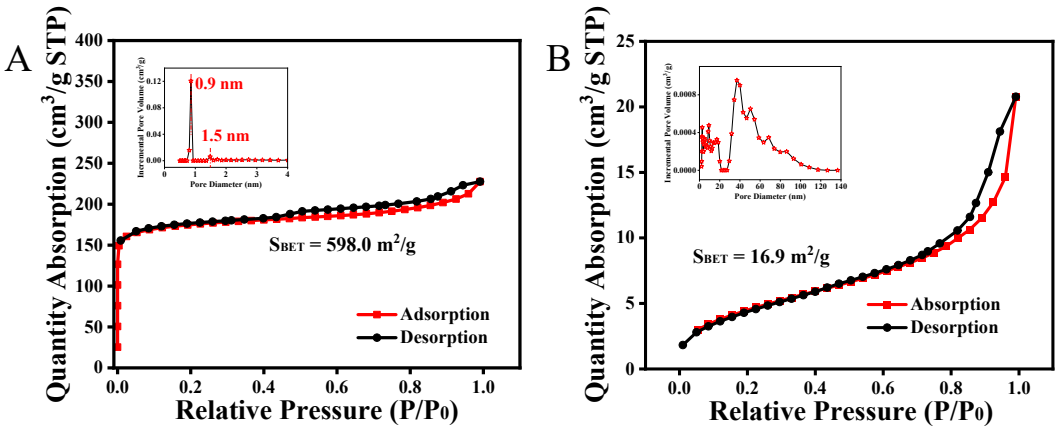

Figure S11. N_2-adsorption-desorption isotherms of (A) Pt-Bi/Cu-MOF and (B) Pt-Bi/CuO samples. The insets represent the corresponding pore size distributions.

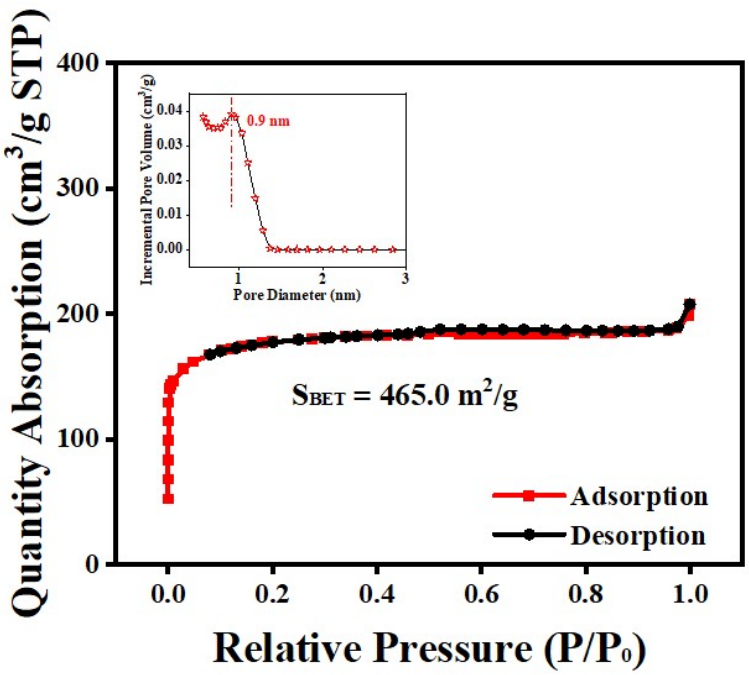

Figure S12. N_2-adsorption-desorption isotherms of Cu-MOF samples. The insets represent the corresponding pore size distributions.

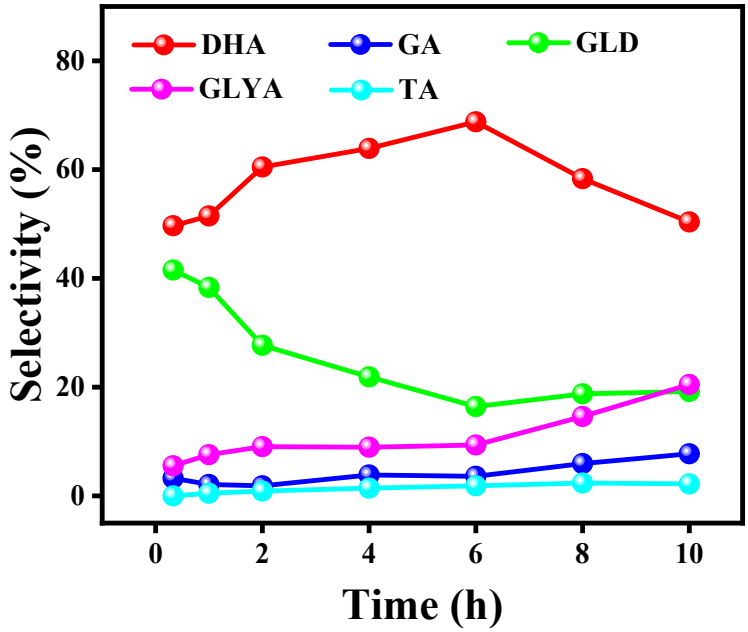

Figure S13. The relationship between the product selectivity and reaction time over Pt-Bi/Cu-MOF.

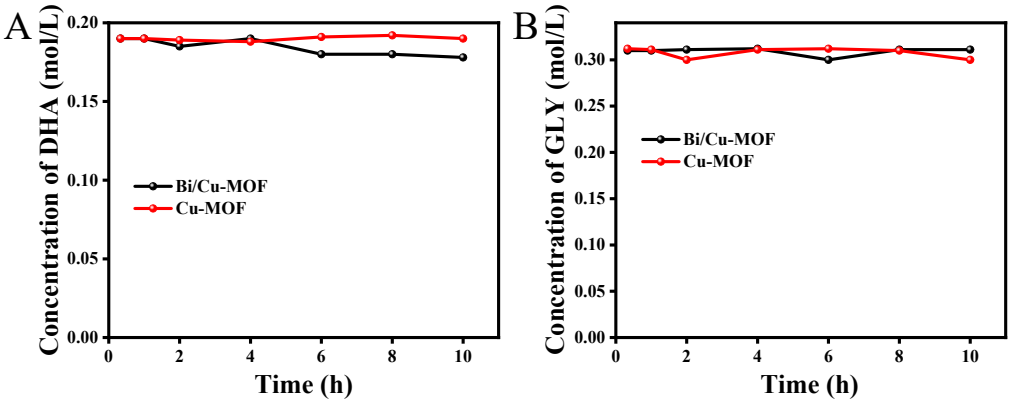

Figure S14. Oxidation of (A) DHA and (B) glycerol over Bi/Cu-MOF and Cu-MOF.

Reaction conditions: catalyst 59 mg, 90 °C.

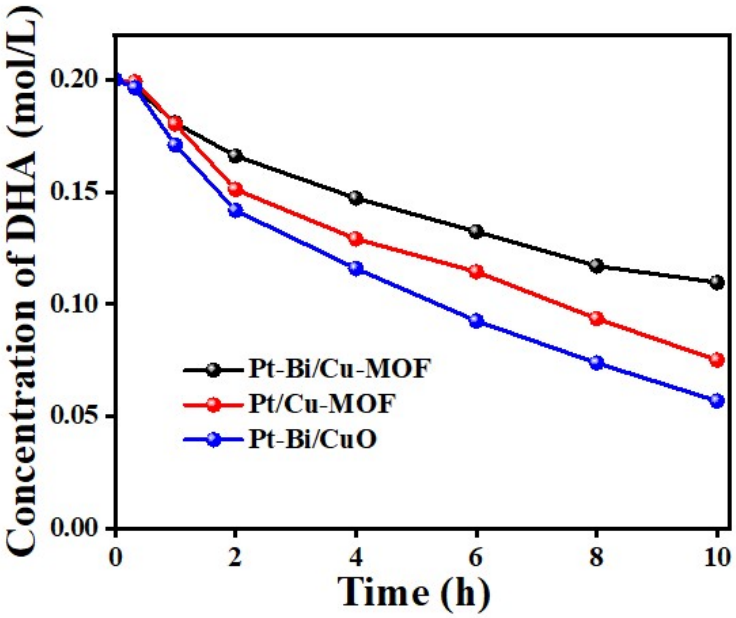

Figure S15. Stability of DHA over Pt-Bi/Cu-MOF, Pt/Cu-MOF, and Pt-Bi/CuO. Reaction conditions: catalyst 59 mg, 90 °C.

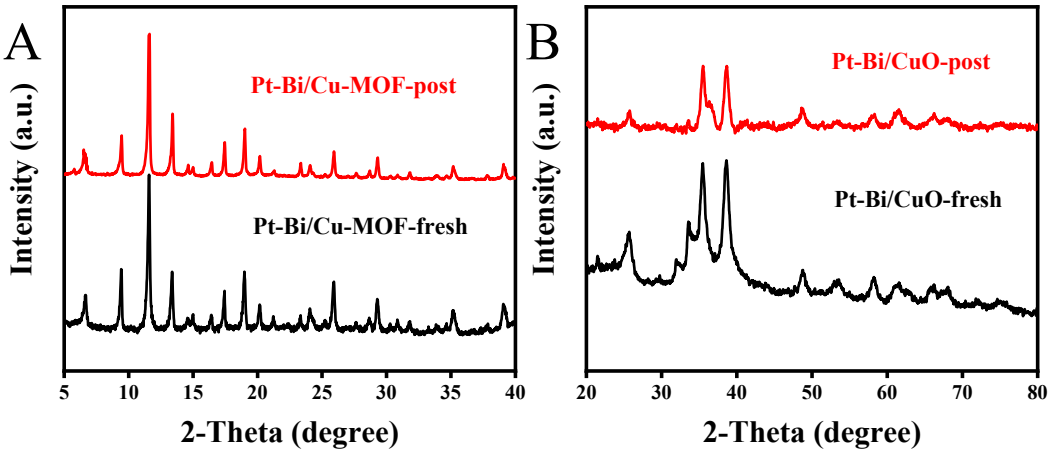

Figure S16. The XRD patterns of Pt-Bi/Cu-MOF and Pt-Bi/CuO before and after catalytic cycles.

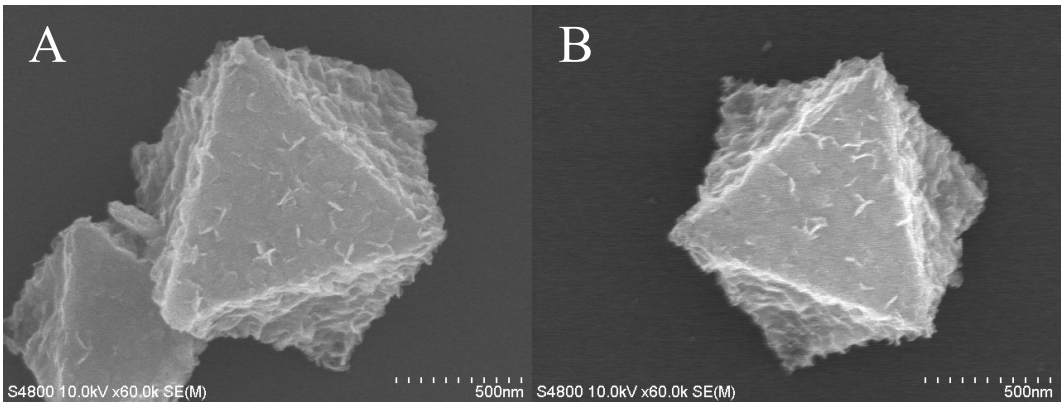

Figure S17. SEM images of Pt-Bi/Cu-MOF catalyst after reaction cycles.

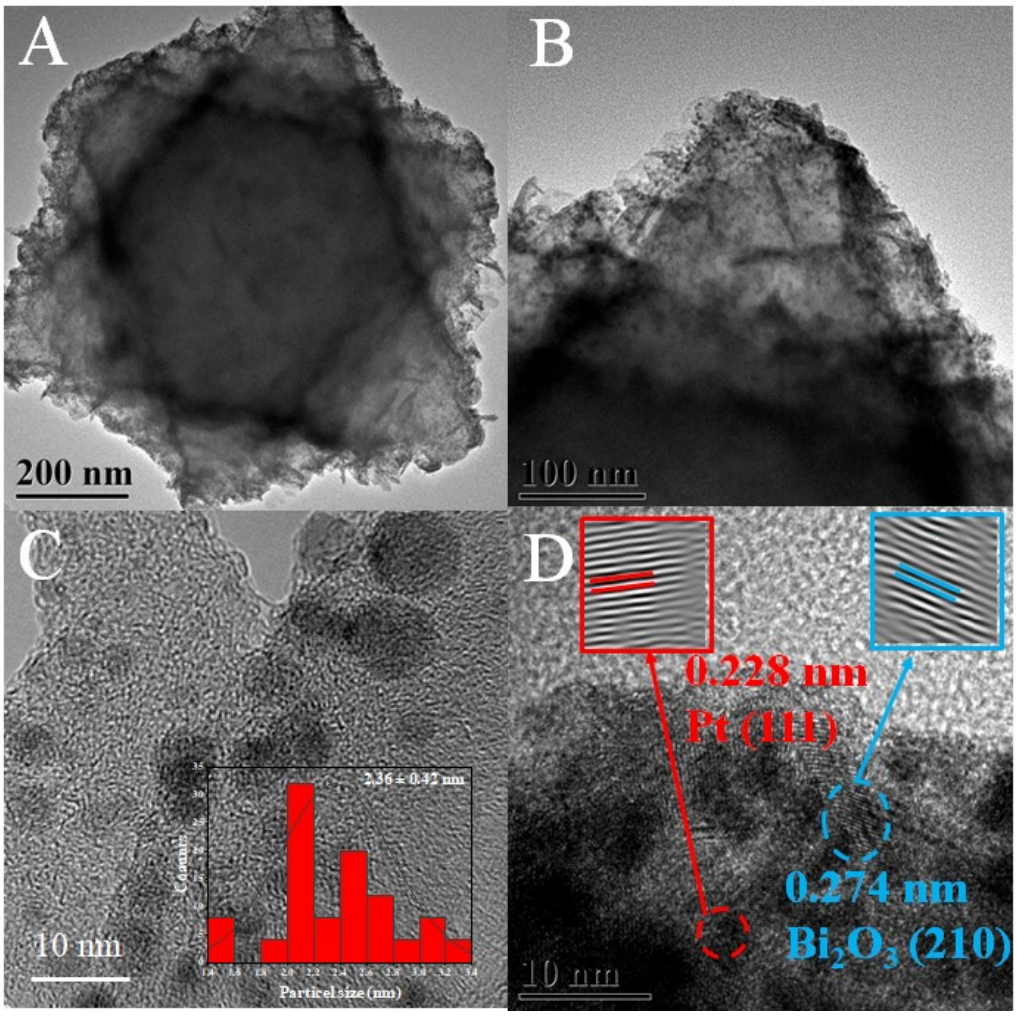

Figure S18. TEM images of Pt-Bi/Cu-MOF catalyst after cycles. The inset in (C) represents the size histogram of Pt nanoparticles.

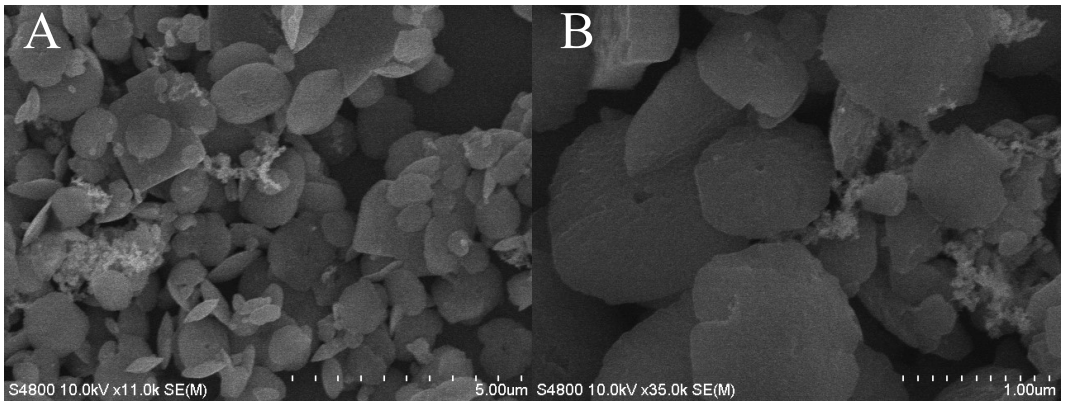

Figure S19. SEM images of Pt-Bi/CuO catalyst after reaction cycles.

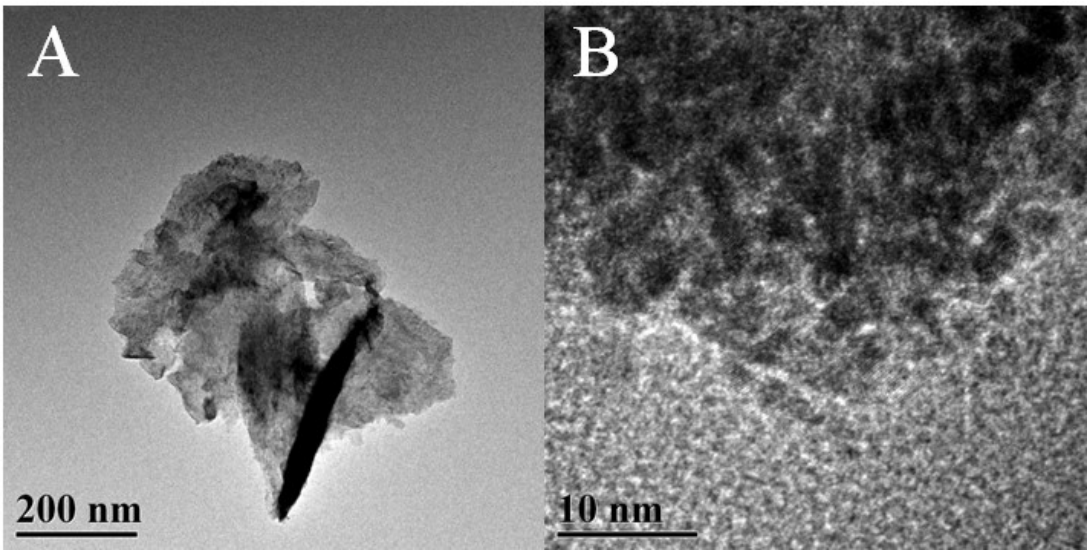

Figure S20. TEM images of Pt-Bi/CuO catalyst after reaction cycles.

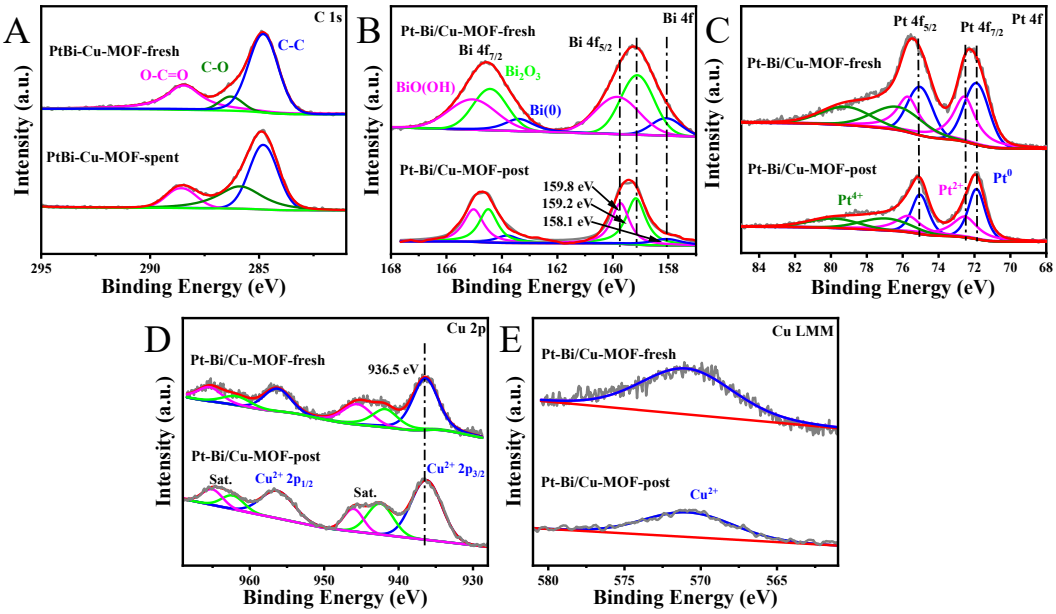

Figure S21. The XPS spectra of (A) C 1s, (B) Bi 4f, (C) Pt 4f, (D) Cu 2p, and (E) Cu LMM for Pt-Bi/Cu-MOF catalyst before and after cycling.

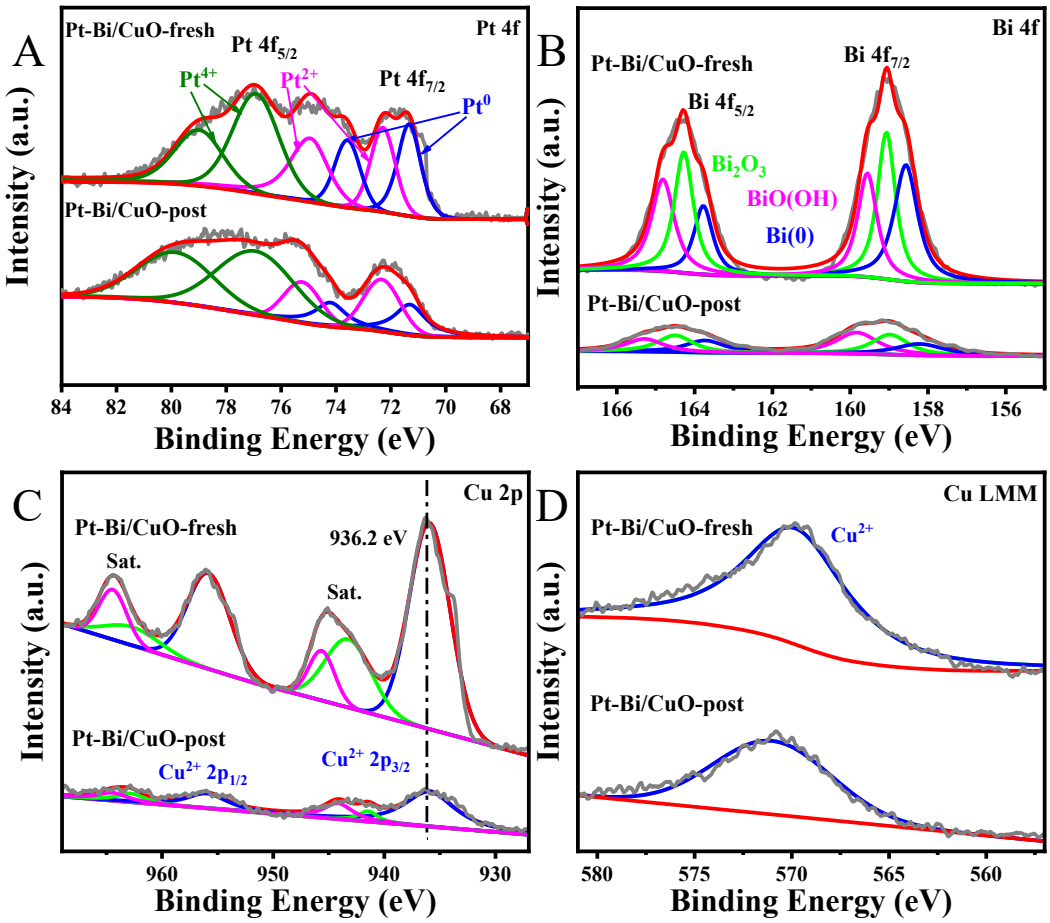

Figure S22. The XPS spectra of (A) Pt 4f, (B) Bi 4f, (C) Cu 2p, and (D) Cu LMM for Pt-Bi/CuO catalyst before and after cycling.

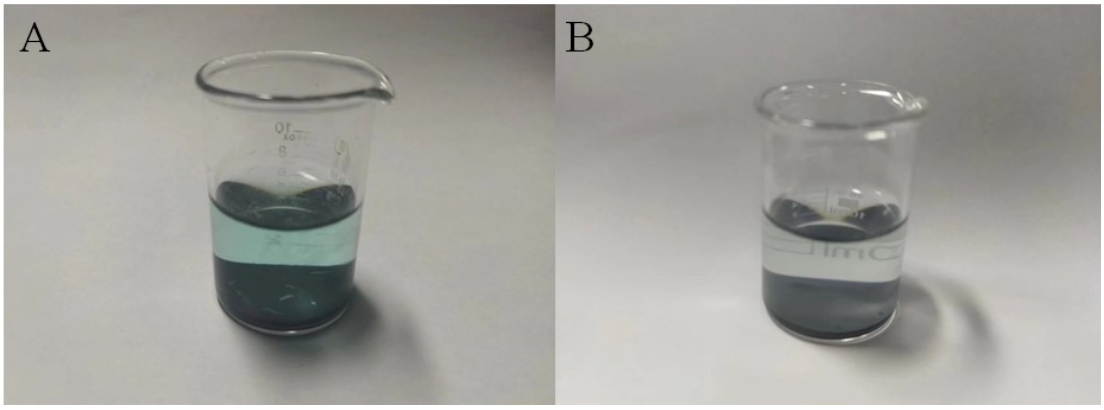

Figure S23. The color change in the glycerol solution after the reaction with (A) Pt-Bi/CuO and (B) Pt-Bi/Cu-MOF catalysts.

Table S3. Comparison of the glycerol-to-DHA performance over the catalysts.

Catalysts	Potency and temperature	Reaction time	Conv. (%)	S. of DHA (%)	Carbon balance (%)	Y. of DHA (%)	Ref
Pt-Bi/Cu-MOF	0.3 M glycerol, 90 °C	6 h	94.2	68.8	97	62.9	This work
Pt/NCNT+Bi(NO_3)·5H_2O	0.1 M glycerol, 60 °C	6 h	29.3	64.4	100.0	★18.9	[1]
5%Pt-5%Bi/C	1 M glycerol, 60 °C	6 h	91.5	49.0	94.0	42.1	[2]
Pt-Bi/SBA-15	0.2 M glycerol, 30 °C	15 h	62.8	40.9	88.0	22.6	[3]
Pt-Bi/HT	1 M glycerol, 60 °C	6 h	25.1	80.6	100.0	★20.2	[4]
Pt/0.1Bi@NC	0.1 M glycerol, 30 °C	15 h	86.8	87.0	90.0	67.9	[5]
Pt/CeO_2-ZrO_2-Bi_2O_3-SnO_2/SBA-16	1 wt% glycerol, 30 °C	4 h	74.0	72.0	100.0	★54	[6]
PtSb/MWCNTs	0.1 M glycerol, 60 °C	-	90.0	51.4	91.0	42.1	[7]
Sb@$PtSb_2$/NC	2 M glycerol, 60 °C, 6 atm O_2	3 h	65.3	39.2	100.0	★25.6	[8]
Au/Cu-NPC-15%-H_2	0.1 M glycerol, 60 °C	4 h	65.6	92.1	98.0	59.2	[9]
AuSiO_2-550	0.25 M glycerol, 140 °C, 30 atm O_2	8 h	16.5	55.1	100.0	★9.1	[10]
0.98wt%Au/$Zn_{2.15}Ga_{1.0}$-LDH	0.1 M glycerol, 60 °C, 5 atm O_2	4 h	72.9	63.8	97.0	45.1	[11]
AuPd/ZnO–CuO	1 M glycerol, 75 °C, 4 atm O_2	4 h	78.2	86.0	97.5	65.5	[12]
Cu(II)-cat	5 g glycerol, 100 mL 3% H_2O_2, 60 °C	4 h	40.3	52.9	100.0	★21.3	[13]
Bi_2O_3/TiO_2	0.5 M Na_2SO_4, 0.1 M glycerol, 25 °C, 0.1 V	10 h	50.0	75.4	100.0	★37.7	[14]

★: The production of DHA is estimated only based on the conversion and selectivity, without the carbon balance correction.

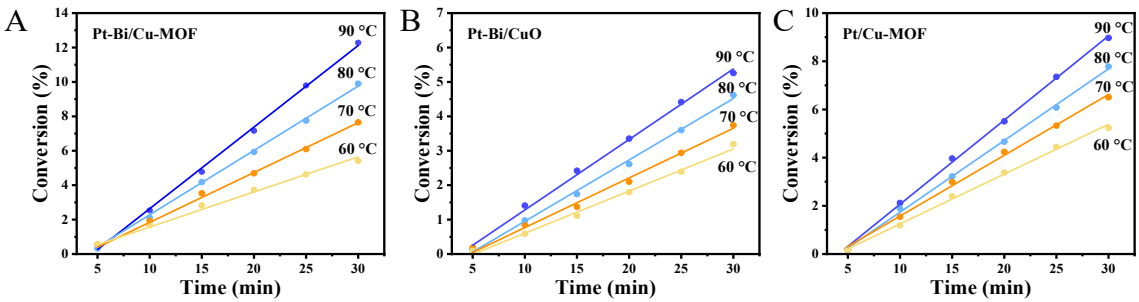

Figure S24. Kinetic studies of glycerol oxidation reactions catalyzed by (A) Pt-Bi/Cu-MOF, (B) Pt/Cu-MOF, and (C) Pt-Bi/CuO. Reaction conditions: 90 °C, 0.5 M glycerol solution, n(glycerol): n(metal) = 200, oxygen supplied under atmospheric pressure.

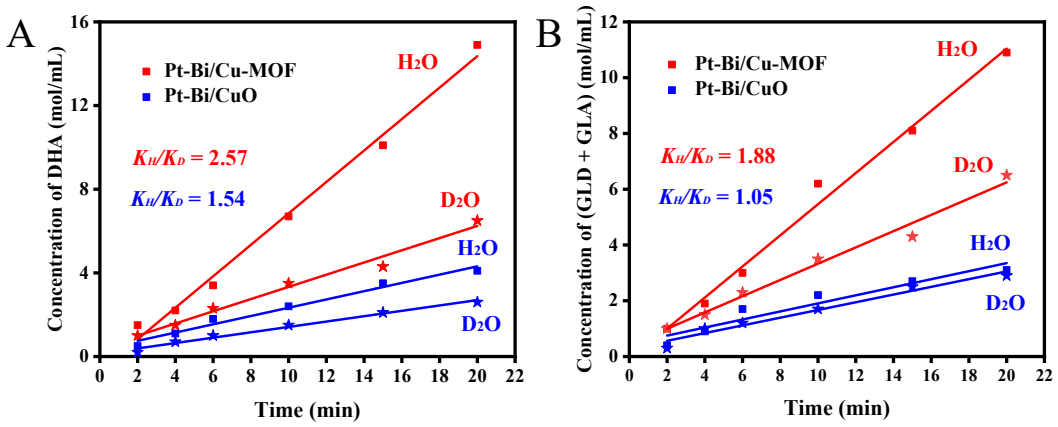

Figure S25. Concentration evolution of (A) DHA and (B) GLD + GLA over Pt-Bi/Cu-MOF and Pt-Bi/CuO catalysts in H_2O or D_2O.

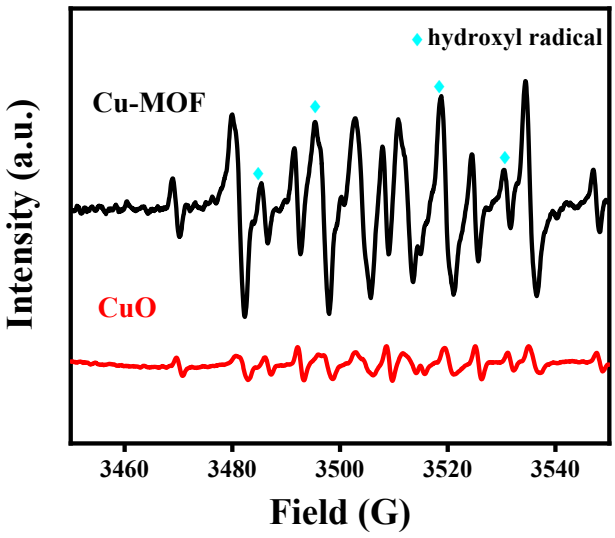

Figure S26. Room-temperature electron paramagnetic resonance spectra of Cu-MOF and CuO in water.

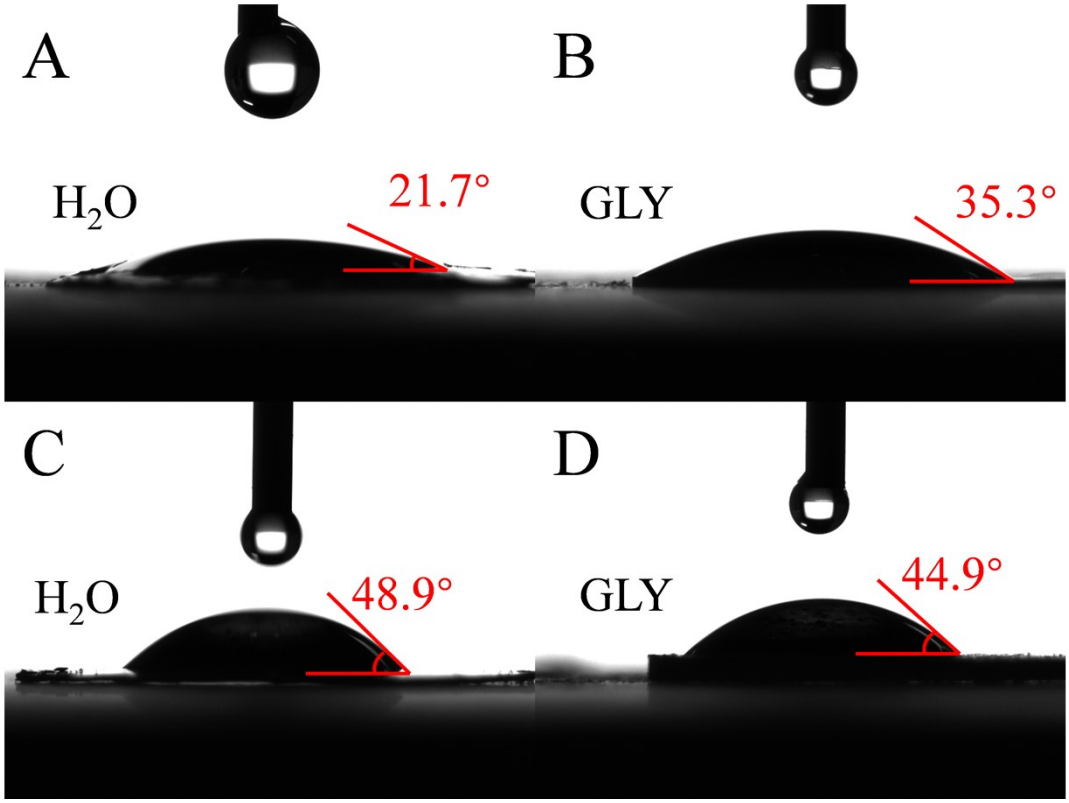

Figure S27. Photos of contact angle experiments. (A, B) Pt-Bi/Cu-MOF, (C, D) Pt-Bi/CuO.

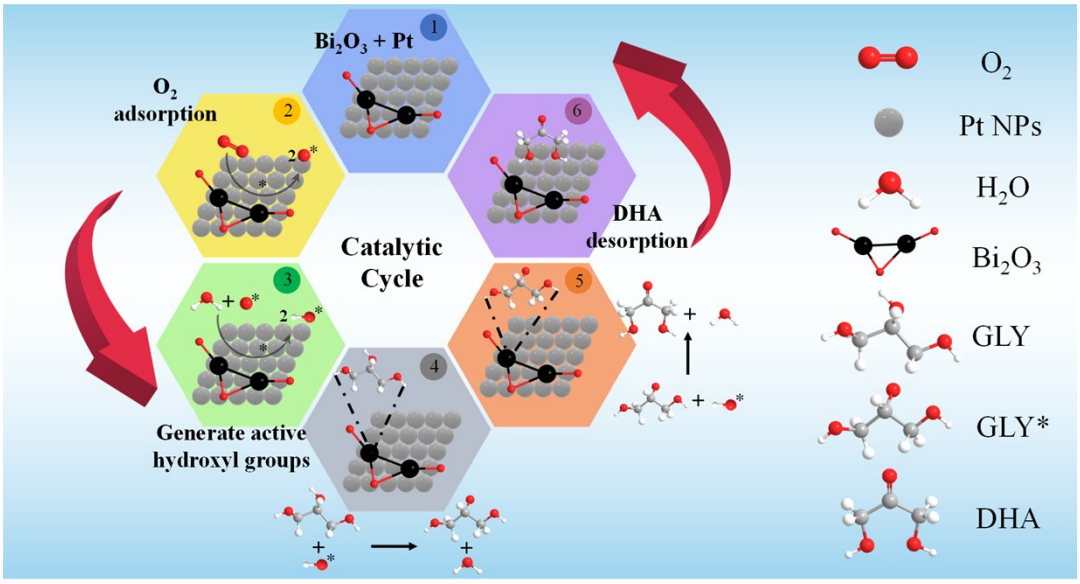

Figure S28. Proposed catalytic cycle of Pt-Bi for DHA formation from glycerol.

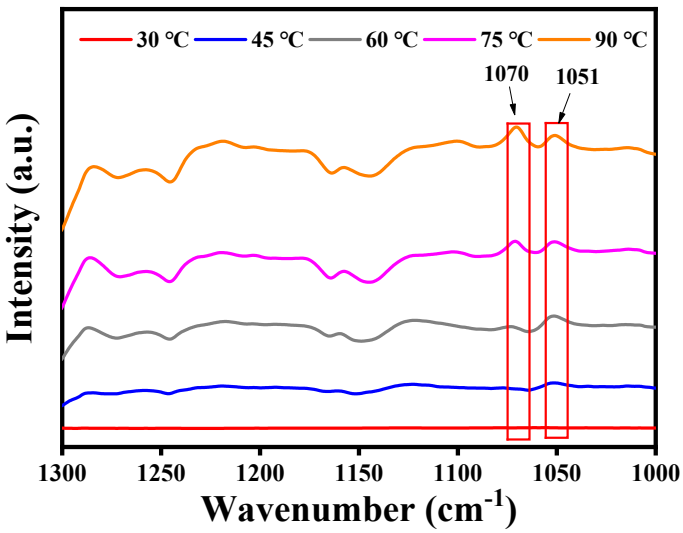

Figure S29. In situ FTIR spectra of glycerol oxidation on Bi/Cu-MOF.

REFERENCES

1. X. M. Ning, Y. H. Li, H. Yu, F. Peng, H. J. Wang and Y. H. Yang, *J. Catal*. **2016**, *335*, 95-104.

2. D. Liang, S. Y. Cui, J. Gao, J. H. Wang, P. Chen and Z. Y. Hou, *J. Catal.,* **2011**, *32*, 1831-1837.

3. S. X. Feng, J. Yi, H. Miura, N. Nakatani, M. Hada and T. Shishido, *ACS Catal.* **2020**, *10*, 6071-6083.

4. W. J. Xue, Z. L. Wang, Y. Liang, H. Xu, L. Liu and J. X. Dong, *Catalysts.* **2018**, *8*, 20-32.

5. N. Huang, Z. H. Zhang, Y. B. Lu; J. S. Tian, D. Jiang, C. G. Yue, P. B. Zhang, P. P. Jiang and Y. Leng, *J. Mater. Chem. A*, **2021**, *9*, 25576-25585.

6. N. Nunotani, M. Takashima, P. G. Choi, Y. B. Choi, *J. Asian. Ceram. Soc*. **2020**, *8*, 470-475.

7. R. F. Nie, D. Liang, L. Shen, J. Gao, P. Chen and Z. Y. Hou, *Appl. Catal. B Environ*. **2012**, *127*, 212-220.

8. L. H. Yang, T. Q. He, C. J. Lai, P. Chen and Z. Y. Hou, *Chinese. J. Catal*, **2020**, *41*, 494-502.

9. H. Tan, C. J. Yao, T. Zhan, W. Q. Li, J. P. Zhu, G. Wang, W. B. Liu, M. T. Sun and S. H. Wang, *Mol. Catalysis*. **2020**, *498*, 11124-11134.

10. V. Margot, V. Vykoukal, A. Styskalik, A. S. Malik, C. Aprile and D. Debecker, *ACS Appl. Nano Mater.* **2022**, *5*, 18977-18985.

11. Z. An, H. H. Ma, H. B. Han, Z. Y. Huang, Y. T. Jiang, W. L. Wang, Y. R. Zhu, H. Y. Song, X. Shu, X. Xiang and J. He, *ACS Catal*. **2020**, *10*, 12437-12453.

12. G. Q. Zhao, G. D. Wu, Y. N. Liu, Y. F. He, J. T. Feng and D. Q. Li, *Catal. Sci. Technol*., **2020**, *10*, 6223-6234.

13. J. Luo, H. G. Li, N. Zhao, F. Wang and F. K. Xiao, *J. Fuel. Chem. Tech*, **2015**, *43*, 677-683.

14. L. Luo, W. S. Chen, S. M. Xu, J. R. Yang, M. Li, H. Zhou, M. Xu, M. F. Shao, X. G. Kong, Z. H. Li and H. H. Duan, *J. Am. Chem. Soc*. **2022**, *144*, 7720-7730.